CHEMICAL ENGINEERING TRANSACTIONS
VOL. 88, 2021
A publication of AIDIC
The Italian Association of Chemical Engineering
Online at www.cetjournal.it
Guest Editors: Petar S. Varbanov, Yee Van Fan, Jiří J. Klemeš

ISBN 978-88-95608-86-0; **ISSN** 2283-9216
DOI: 10.3303/CET2188040

Thermo-Economic Evaluation of Thermocline Thermal Energy Storage Tank for CSP Plants

Karem Elsayed Elfeky*, Abubakar Gambo Mohammed, Qiuwang Wang

Key Laboratory of Thermo-Fluid Science and Engineering, MOE, Xi'an Jiaotong University, Xi'an, Shaanxi 710049, China
wangqw@mail.xjtu.edu.cn

A thermal energy storage (TES) approach is the primary technology for ensuring the continuous supply of electricity from solar power plants. In solar power research and development, selecting the best storage device and the right thermal storage content remains a major challenge. As compared to the liquid storage substance in a two-tank TES system, the thermocline TES system is a more cost-effective alternative for storing sensible heat. Centred on the concept of using a thermocline tank in concentrated solar power plants, the current study utilizes a range of solid storage materials as filling materials, with air acting as the heat transfer fluid. The major contribution of this research is to directly compare the thermo-economic efficiency potential of four storage materials (Quartzite, BOF-slag, Magnetite, and River rock) used in the thermocline storage tank in order to meet some design criteria of a CSP plant without the need for parametric studies. The thermo-economic performance of an air rock thermocline TES tank was investigated using a discrete element system combined with a numerical approach of computational fluid dynamics. The Quartzite presents the highest overall efficiency of 70 %, followed by the River rock with 61 %, and BOF-Slag equals 54 %, while Magnetite is the least in a row with 52 % overall efficacy. Based on thermal-economic performance evaluation, the results showed that the storage capacity of the Quartzite is greater by 37.5 %, 51.2 %, 21.2 % than BOF-Slag, River rock, and Magnetite.

1. Introduction

Solar energy has become one of the main energy sources to fulfil the global energy demand, minimize fuel consumption, and avoid carbon dioxide emissions from increasing (Richter et al., 2021). The intermittent nature of solar energy needs an energy storage subsystem to use the energy source effectively. Solar thermal power technologies, such as concentrating solar power (CSP) plants systems, collect the thermal energy of the sun and convert it into electricity through a heat engine linked to a generator (Pramanik and Ravikrishna, 2017). One of the key elements of CSP is the capacity to store energy effectively and cost-effectively (Li and Ju, 2018). In the air rock thermocline tank, the solar thermal energy storage (TES) is productive and adequate for CSP use (Hoivik et al., 2019).

In recent times, scholars have been interested in the topic of TES using packing rocks. The heat capacity and conductivity are by far the most critical elements of storage materials; however, conductivity has less impact (Hänchen et al., 2011). The thermal behaviour of the thermocline storage tank, which is examined during the recharging and discharging periods, is designed to enhance the heat transfer mechanism (Elfeky et al., 2018). Rao et al. (2019) proposed three solid sensible heat storage models lab performance analysis. The results revealed that the discharge efficiency was significantly improved, and the discharge time decreased because of the use of embedded fins. In a previous study, the thermal efficiency of a scale model of an air rock thermocline TES tank was investigated using a discrete element system (DEM) combined with a numerical model of computational fluid dynamics (CFD) (Elfeky et al., 2021). The study is carried out to optimize the TES thermocline tank's thermal behaviour by changing the heat transfer fluid (HTF) inlet velocity. In a related paper, Tiskatine et al. (2017) examined the impact of the variance of axial porosity and how to choose a convenient storage medium for the TES packing device. Findings showed that axial porosity variation affected the temperature profiles for the charging/discharging cycles and pressure drop. The first study was carried out to investigate the heat transfer coefficients in a porous medium filled with rocks by Löf et al. (1984). The

Paper Received: 19 June 2021; Revised: 3 July 2021; Accepted: 4 October 2021
Please cite this article as: Elfeky K.E., Mohammed A.G., Wang Q., 2021, Thermo-Economic Evaluation of Thermocline Thermal Energy Storage Tank for CSP Plants, Chemical Engineering Transactions, 88, 241-246 DOI:10.3303/CET2188040

enhancement in heat transfer rate is determined by mass flow and particle size, whereas the inlet temperature does not have a direct influence. A 1 MWe CSP plant's thermal output was investigated by Cocco et al. (2015) with direct and indirect TES modules. The study found that the two-tank TES efficiency is higher than the thermocline TES tank, but that employing a thermocline TES reservoir reduces the cost of energy generation for CSP facilities. In earlier findings, the fluid flow and heat transfer processes of an air rock thermocline TES tank were investigated (Elfeky et al., 2020). The aim of this research is to see how changing the Reynolds number affects the thermal behaviour of the TES thermocline tank.

Based on the above literature review, it can be noted that most of the previous numerical studies lack clear knowledge of the process of the heat transfer between HTF and the filler material in detail. For instance, the influence of the storage material type on the increase/decrease of the temperature of the filler material during the charging/discharging cycles. In addition, the impact of the storage material type on the absorbed and recovered of thermal energy, especially considering the thermo-economic efficiency potential of four different storage materials. In the present study, the thermo-economic efficiency potential of four storage materials (Quartzite, BOF-slag, Magnetite, and River rock) used in the thermocline storage theory is highlighted for the charging/discharging cycles. The current article describes the development of an innovative method for investigating the thermal performance of the thermocline storage tank, which is used in solar tower power plants, a technology that is aimed at energy conservation, the optimal use of energy resources, the optimization of energy processes, and sustainable energy systems.

2. Model formulation

2.1 Physical model

The TES device for packaged beds has demonstrated its efficiency through energy storage due to its high thermal performance as compared to a two-tank storage system during charge/discharge cycles. The arrangement of the TES tank prototype is shown schematically in Figure 1. The aspect ratio (H_{tank}/D_{bed}) of the tank is 4.287, comparable to that used in CSP applications (Zanganeh et al., 2015). The TES thermocline system comprises a vertical tank with two dispensers, one at the entrance and one at the exit, as can be seen in Figure 1. For the charge cycle, the hot air at a higher temperature (T_h) passes from the top section of the TES tank, delivers energy to the solid medium, and exits from the lower section. While during the discharge process, the cold air (T_c) moves from the bottom of the TES tank at a lower temperature, accumulates heat from the solid medium and leaves through the top section. The height of the packaged bed area is H_{bed}, while D_{bed} is the tank diameter. The average porosity of 515 spheres is used in the TES tank system denoted by ϕ. Table 1 displays the geometric properties of the packaging models.

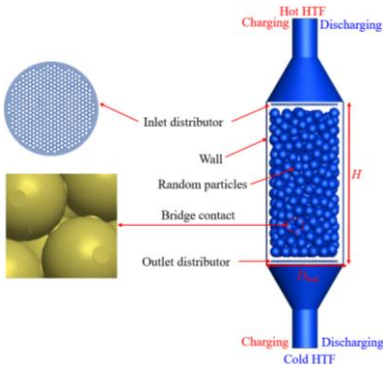

Figure 1: Schematic structure of the TES tank

Table 1: Thermocline TES tank geometric variables

Parameters	Values	Parameters	Values
H_{tank} (m)	0.171	d_s (m)	0.006
H_{bed} (m)	0.08	T_h (°C)	650
D_{bed} (m)	0.04	T_c (°C)	350
ϕ (-)	0.417	HTF	Air

The DEM approach is used in this analysis for generating 515 spheres (Bai et al., 2009). By using the EDEM program, the solid spherical particles fall to the bottom of the tank by gravity until the tank is completely filled. A balance is created for all the forces that effect the solid sphere during falling, including the force of gravity, the

force between spheres as well as the force between spheres and the wall of the tank. The DEM simulation is stopped during the generation of solid spheres when the final state is reached, which means that the velocity of all spheres is approximately equal to zero.

2.2 Governing equations and computing procedures

The fluid flow is unsteady and incompressible in this analysis. The fluid dynamics and temperature variations during the charging/discharging processes are represented using the 3D Navier-Stokes's equations and energy balance. In this analysis, the particle Reynolds number (Re_p) changes from 400 to 1,600, implying that the flow inside the tank is turbulent, as stated in (Yang et al., 2010). To investigate turbulent flow in porous media, the RNG k- ε turbulence approach has been suggested, particularly for small eddies that are independent of larger phenomena (Yang et al., 2010). For mass, momentum, and energy, the equations of conservation are as follows:
Continuity:

$$\frac{\partial \rho}{\partial t} + \rho(\nabla \cdot \vec{V}) = 0 \tag{1}$$

Momentum:

$$\rho_f \left[\frac{\partial \vec{V}}{\partial t} + (\vec{V} \cdot \nabla \vec{V}) \right] = \rho g - \nabla p + \nabla \cdot [(\mu_f + \mu_t)(\nabla \vec{V} + (\nabla \vec{V})^T)] \tag{2}$$

Energy:

$$\rho_f \left[\frac{\partial T}{\partial t} + (\vec{V}.\nabla T) \right] = \nabla \cdot [(\frac{k_f}{c_p} + \frac{\mu_t}{\sigma_T}) \cdot (\nabla T)] \tag{3}$$

The transport equations for the RNG k-ε approach are as follows:

$$k : \rho_f \left[\frac{\partial k}{\partial t} + (\vec{V}.\nabla k) \right] = \nabla \cdot [(\mu_f + \frac{\mu_t}{\sigma_k}) \cdot \nabla k] + P_k - \rho_f \varepsilon \tag{4}$$

$$\varepsilon : \rho_f \left[\frac{\partial \varepsilon}{\partial t} + (\vec{V}.\nabla \varepsilon) \right] = \nabla \cdot [(\mu_f + \frac{\mu_t}{\sigma_\varepsilon}) \cdot \nabla \varepsilon] + \frac{c_{\varepsilon 1} \varepsilon}{k} P_k - c_{\varepsilon 2} \rho_f \frac{\varepsilon^2}{k} \tag{5}$$

where P_k is the turbulence shear production, μ_t is the turbulent viscosity, $c_{\varepsilon 1}$ and $c_{\varepsilon 2}$ are constants of the turbulence model in ε equation, σ_T, σ_k and σ_ε are the Prandtl numbers in T, k and ε equations. The relationships of these constants are presented as:

$$P_k = \mu_t \cdot (\nabla \vec{V} + (\nabla \vec{V})^T) : \nabla \vec{V}; \quad \mu_t = \rho_f c_\mu \frac{k^2}{\varepsilon} \tag{6}$$

$$c_{\varepsilon 1} = 1.42 - f_\eta \ (f_\eta = \frac{\eta(1 - \eta / 4.38)}{1 + 0.012\eta^3}, \quad \eta = \frac{P_k}{\rho_f c_\mu \varepsilon}) \tag{7}$$

where the value of c_μ, $c_{\varepsilon 2}$, σ_T, σ_k and σ_ε are 0.085, 1.68, 1.0, 0.718, and 0.718.
In this analysis, the continuity, momentum, and energy equations are solved using the commercial code ANSYS FLUENT 16.0. The SIMPLE algorithm has been used to link the velocities and pressures in conservation equations. The convective terms in the momentum, energy, and turbulence equations are discretized using the second-order upwind scheme. All the equations' residuals are set to be less than 10^{-5}, except for the energy equation, which is set to be less than 10^{-8}.

2.3 Tests of mesh generation and grid independence

The geometry of the thermocline TES tank with 515 spheres is very complicated and thus, in the present work, the geometric model is divided using tetrahedral mesh. To adjust the grid at the contact points, short cylinder bridges are built. This change is made in accordance with the findings of an analysis (Dixon et al., 2012). The test of the grid independence for the thermocline TES tank has been illustrated in lab past work (Elfeky et al., 2020). For the current calculations, a computational element size of 1/20 d_s has been chosen.

3. Results and discussion

The thermal and economic performance of the TES thermocline tank is one of the essential factors for evaluating power production and CSP reliability in the current study. The mechanism of energy storage in the thermocline tank that maintains the CSP plants running and the heat transfer process within this system during the charging and discharging processes is important and will be explored in-depth in this analysis. The performance metrics in terms of charging, discharging, and overall efficiency provide the general indexes for TES design and analysis of the thermocline tank. All these parameters have been defined in lab previous work (Elfeky et al., 2018).

3.1 Axial temperature allocation

Figure 2 shows the HTF and storage material temperature distribution for different storage material (Quartzite, BOF-slag, Magnetite, and River rock) types during charge and discharge processes. It is clear that the behaviour of the storage materials in the TES tank is influenced by its thermo-physical characteristics. The Quartzite is the fastest to charge, followed by River rock, then BOF-slag. The higher the temperature difference between the HTF and the storage material, the larger the heat transfer rate. The thermo-physical characteristics of Quartzite better fit the heat transfer temperature profile. This increases the heat transfer rate and the dynamic efficiency of the system. Quartzite obtained the highest thermal efficiency after 200 s of charging and discharging cycles, as shown in Figure 2, allowing it to store and release as much energy as possible in contrast with all other cases studied. The configuration of the Quartzite is roughly the best scenario for this, as the TES tank system can store and release the most energy. The charge temperature was reached by more than 75 % of the height of the TES thermocline tank in the Quartzite scenario. After the same time frame, the BOF-slag, Magnetite, and River rock configurations reached 60 %, 65 %, and 74 % of the height of the TES thermocline tank to the charge temperature. Furthermore, the Quartzite case has the highest thermal efficiency, while the River rock case comes in second during the discharging period.

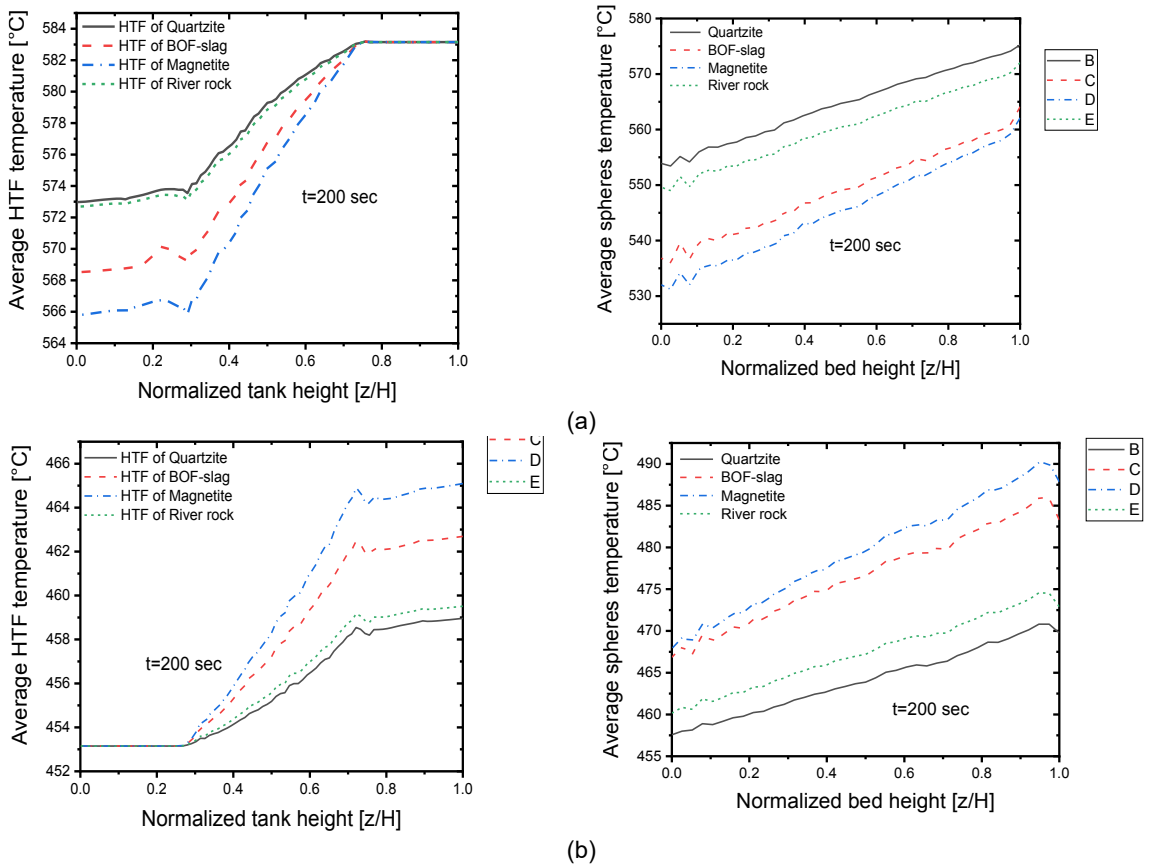

Figure 2: Comparison of HTF and storage material temperature allocation a) Charge and b) Discharge cycles

Figure 3 shows the stored energy, while Figure 4 illustrates the charging, discharging, and overall performance efficiency for each configuration. The results show that the accumulated energy of Quartzite is greater by 25.5 %, 51.4 %, and 21.2 % than BOF-Slag, River rock, and Magnetite, respectively, at the end of the charging period, as shown in Figure 3. As shown in Figure 2, the Quartzite case has the best temperature match between storage material and HTF. The results show that by using air as the HTF, the overall storage performance varies between 70 % and 52 %. Quartzite has the highest overall efficiency of 70 %, followed by River rock with 62 % and BOF-Slag with 55 %, while Magnetite has the lowest overall efficacy of 52 %. Because of its higher thermal conductivity, Quartzite has a higher efficiency, which is important given the short discharge time.

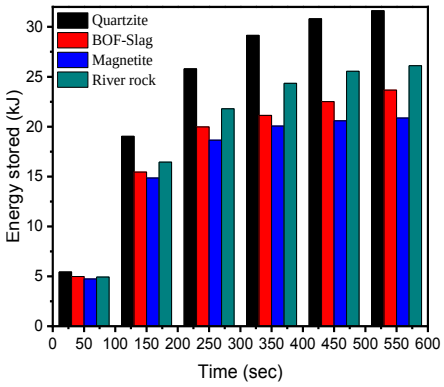

Figure 3: Total energy stored vs. time for different storage material

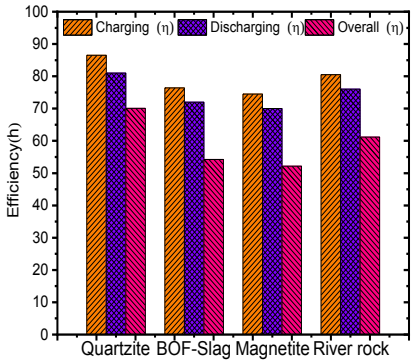

Figure 4: The thermal performance analysis

Figure 5 indicates the overall storage capacity of the TES thermocline tank in the structures studied. During the charging and discharging cycles, the analysis indicate that the storage capacity of the Quartzite is greater by 37.5 %, 51.4 %, 21.2 % than BOF-Slag, River rock, and Magnetite, respectively. The maximum values of thermal conductivity of Quartzite also favor higher overall efficiency. This may also explain why Magnetite, which has the least efficient thermal properties, has lower efficiency. Furthermore, as shown in Figure 6, the capacity cost of the BOF-Slag is the lowest of all the studied cases, making it the best option for economic feasibility. Quartzite has a capacity cost of 17.5 $ per kWh and a storage capacity of 31.3 kJ. In contrast to Quartzite, BOF-Slag has a lower capacity cost of 10 $ per kWh. As predicted, the BOF-slag case has the lowest TES system capacity cost. Quartzite is more economically advantageous than River rock, despite its higher price. This is mainly due to the high thermal conductivity, which results in a smaller tank volume, lowering the cost of construction materials and HTF. As a consequence, the thermophysical properties of storage products, as well as the price of the commodity, play a significant role in the economic analysis.

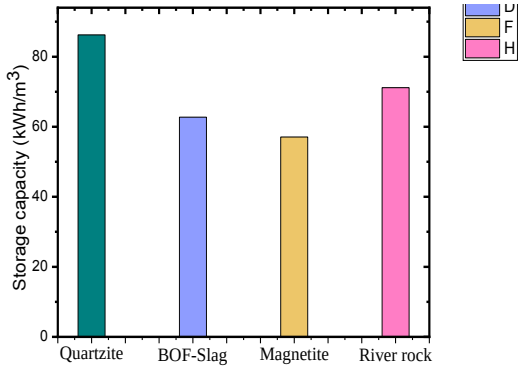

Figure 5: Storage capacity of the four different cases'

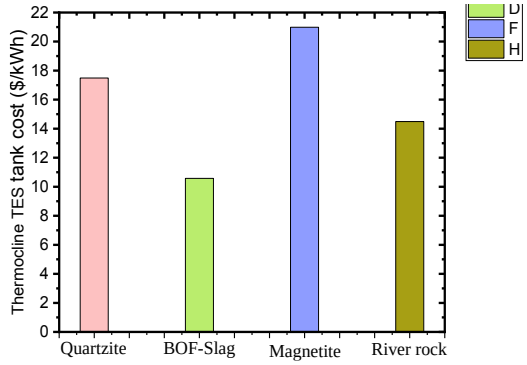

Figure 6: The capacity cost ($/kWh) for four different types of storage material

4. Conclusions

The current study utilizes a range of solid storage materials as filling materials, with air acting as the heat transfer fluid. The thermo-economic efficiency potential of four storage materials (Quartzite, BOF-slag, Magnetite, and River rock) used in the thermocline storage are determined in this research. The thermo-economic performance of an air rock thermocline TES tank was investigated using a DEM combined with a numerical approach of CFD. Using BOF-Slag as a solid filler inside a thermocline TES has a number of benefits, including reducing the environmental effect of fossil fuels and increasing the ability of renewable energy technologies such as concentrated solar power and energy recovery systems. It also has acceptable thermo-physical properties and good thermal activity within the TES, making it economically competitive. The results presented show that with air as HTF, the overall storage efficiency is ranged between 70 % and 52 %. Based on thermal-economic performance evaluation, the results showed that the storage capacity of the Quartzite is greater by 37.5 %, 51.2

%, 21.2 % than BOF-Slag, River rock, and Magnetite. The capacity cost and the storage capacity of the Quartzite are 17.5 $/kWh, and 31.3 kJ, respectively. While, BOF-Slag has a slightly lower capacity cost of 10 $/kWh as compared to the Quartzite. This work can be extended by investigating the capacity ratio and the utilization ratio of the air rock thermocline storage tank to optimize its thermal-economic performance which is used in CSP plants.

Acknowledgments

This work is financially supported by the Fundamental Scientific Research Expenses of Xi'an Jiaotong University (xzy012021021), Foundation for Innovative Research Groups of the National Natural Science Foundation of China (No.51721004) and the 111 Project (B16038).

References

Bai H., Theuerkauf J., Gillis P.A., Witt P.M., 2009, A coupled DEM and CFD simulation of flow field and pressure drop in fixed bed reactor with randomly packed catalyst particles, Industrial & Engineering Chemistry Research, 48, 4060 - 4074.

Cocco D., Serra F., 2015, Performance comparison of two-tank direct and thermocline thermal energy storage systems for 1 MWe class concentrating solar power plants, Energy, 81, 526 - 536.

Dixon A.G., Walls G., Stanness H., Nijemeisland M., Stitt E.H., 2012, Experimental validation of high Reynolds number CFD simulations of heat transfer in a pilot-scale fixed bed tube, Chemical Engineering Journal, 200, 344 - 356.

Elfeky, K.E., Mohammed, A.G., Wang, Q.W, 2021, Performance analysis of an air rock thermocline TES tank for concentrated solar power plants using the coupled DEM–CFD approach, Clean Technologies and Environmental Policy, 1 - 17.

Elfeky, K.E., Mohammed, A.G., Wang, Q.W., 2020, Investigate the Thermal Performance of Thermocline Tank for Hybrid Solar Tower Power Plants, Chemical Engineering Transactions, 81, 523 - 8.

Elfeky, K.E., Mohammed, A.G., Wang, Q.W., 2020, Numerical investigation of cycle cut-off criterion on system performance of thermocline TES tank for CSP plants. Chemical Engineering Transactions, Chemical Engineering Transactions, 81, 499 - 504.

Elfeky K.E., Ahmed N., Wang Q.W., 2018, Numerical comparison between single PCM and multi-stage PCM based high temperature thermal energy storage for CSP tower plants, Applied Thermal Engineering, 139, 609 - 622.

Hänchen M., Brückner S., Steinfeld A., 2011, High-temperature thermal storage using a packed bed of rocks-heat transfer analysis and experimental validation, Applied Thermal Engineering, 31,1798 - 1806.

Hoivik N., Greiner C., Barragan J., Iniesta A.C., Skeie G., Bergan P., Blanco-Rodriguez P., Calvet N., 2019, Long-term performance results of concrete-based modular thermal energy storage system, Journal Energy Storage, 24, 100735.

Li B., Ju F., 2018, Thermal stability of granite for high temperature thermal energy storage in concentrating solar power plants, Applied Thermal Engineering, 138, 409 - 416.

Löf G.O.G., Hawley R.W., 1948, Unsteady-state heat transfer between air and loose solids, Industrial Chemical Engineering, 40, 1061- 1070.

Pizzolato A., Donato F., Verda V., Santarelli M., Sciacovelli A., 2017, CSP plants with thermocline thermal energy storage and integrated steam generator–Techno-economic modeling and design optimization, Energy, 139, 231 - 246.

Pramanik S., Ravikrishna R.V., 2017, A review of concentrated solar power hybrid technologies, Applied Thermal Engineering, 127, 602 - 637.

Richter P., Trimborn T., Aldenhoff L., 2021, Predictive storage strategy for optimal design of hybrid CSP-PV plants with immersion heater, Solar Energy, 218, 237 - 50.

Rao C.R.C., Vigneshwaran K., Niyas H., Muthukumar P., 2019, Performance investigation of lab-scale sensible heat storage prototypes, International Journal of Green Energy, 16, 1363 - 1378.

Tiskatine R., Aharoune A., Bouirden L., Ihlal A., 2017, Identification of suitable storage materials for solar thermal power plant using selection methodology, Applied Thermal Engineering, 117, 591 - 608.

Yang J., Wang Q., Zeng M., Nakayama A., 2010, Computational study of forced convective heat transfer in structured packed beds with spherical or ellipsoidal particles, Chemical Engineering Science, 65, 726 - 738.

Zanganeh G., Khanna R., Walser C., Pedretti A., Haselbacher A., Steinfeld A., 2015, Experimental and numerical investigation of combined sensible–latent heat for thermal energy storage at 575 °C and above, Solar Energy, 114, 77 - 90.